Printed array of thin-dielectric metal-oxide-metal (MOM) tunneling diodes

Mario Bareiß,[1,a)] Andreas Hochmeister,[1] Gunther Jegert,[1] Ute Zschieschang,[2] Hagen Klauk,[2] Rupert Huber,[3] Dirk Grundler,[3] Wolfgang Porod,[4] Bernhard Fabel,[1] Giuseppe Scarpa,[1] and Paolo Lugli[1]
[1]*Institute for Nanoelectronics, Technische Universität München, 80333 Munich, Germany*
[2]*Max Planck Institute for Solid State Research, Heisenberstr. 1, 70569 Stuttgart, Germany*
[3]*Department of Physics, Technische Universität München, James-Franck-Str. 1, 85745 Garching, Germany*
[4]*Center for Nano Science and Technology, University of Notre Dame, Indiana 46556, USA*

(Received 21 February 2011; accepted 25 June 2011; published online 26 August 2011)

A large area array of metal-oxide-metal (MOM) tunneling diodes with an ultrathin dielectric (~3.6 nm aluminum oxide) have been fabricated via a transfer-printing process. The MOM diodes exhibit an excellent tunneling behavior that is suitable for rectifying high-frequency ac current into direct current (dc). Direct tunneling and Fowler-Nordheim tunneling have been observed over eight orders of magnitude in current density. The ratio between forward and reverse current is as large as two orders of magnitude. Simulations have been carried out to extract the static device parameters and have confirmed the existence of a dipole layer at the aluminum/aluminum oxide interface of the printed tunneling diodes. Capacitance measurements have shown that the permittivity of the ultrathin aluminum oxide film is smaller than that of bulk aluminum oxide. The mechanical yield of the transfer-printing process is better than 80%, confirming that transfer printing is a promising candidate for the efficient fabrication of quantum devices over large areas.
 [doi:10.1063/1.3615952]

I. INTRODUCTION

Dipole antenna-coupled metal-oxide-metal diode detectors have been shown to be very promising for the absorption of electromagnetic radiation in the long-wave infrared (LWIR) band.[1,2] These detectors offer full compatibility with complementary metal oxide semiconductor (CMOS) technology as well as high-speed and uncooled room-temperature operation in a small pixel footprint.[3] The most challenging device in these detectors is the metal-oxide-metal (MOM) tunneling diode as it requires a very thin, defect-free, and compact tunneling oxide. By selecting electrode metals with dissimilar work functions, the tunneling current through the thin dielectric becomes asymmetric with respect to the polarity of the voltage applied across the MOM diode. On this account, MOM tunneling diodes have the potential for excellent rectification at high frequencies.[4] MOM tunneling diodes fabricated by a combination of metal vacuum deposition, natural oxidation, electron-beam lithography, and lift-off techniques have shown very promising performance.[5,6] However, because of long exposure times and poor cost effectiveness, this fabrication method is not suitable for the production of dense arrays of hundreds or thousands of tunneling diodes for imaging devices. An alternative promising fabrication technique is the direct transfer printing. A single metal layer[7] or a stack of different materials (e.g., metals and insulators[8,9]) was prepared on a stamp and then transferred onto a target substrate. Up to now, only stacks with thicknesses in the range of several tens of nanometers have been realized and transferred.[10] For the application discussed here, thinner oxides down to a few nanometers are needed to permit large quantum-tunneling current densities.[11,12]

This article reports the fabrication process of aluminum/aluminum oxide/gold ($Al/AlO_x/Au$) tunneling diodes with a very thin (3.6 nm thick) and compact oxide dielectric, the mechanical yield of the transfer printing process, and the electrical performance of the printed MOM tunneling diodes. The layer stack of the MOM diode structures was deposited onto a suitable stamp, and then the entire diodes were transfer-printed in a single printing step onto the target substrate to allow for the electrical characterization of the devices. Direct tunneling and Fowler-Nordheim tunneling have been observed, and the material characteristics were extracted by comparing the experimental measurements with microscopic simulations based on a kinetic Monte Carlo model.

II. FABRICATION

A silicon wafer covered with a hydrophobic organic self-assembled monolayer (SAM) of perflouroctyltrichlorsilane as an anti-sticking layer is used as a stamp. To create the hydrophobic SAM, the wafer is briefly exposed to an oxygen plasma (to create a density of hydroxyl groups sufficient for molecular self-assembly),[13,14] placed for 30 min into a vacuum chamber along with 0.5 ml of perflouroctyltrichlorsilane at a pressure of 10 mbar, and then annealed at ~140 °C on a hotplate. The SAM coverage reduces the surface energy to 20 mJ/m,[2,15] making the wafer suitable as a stamp. Due to the excellent stability of silane SAMs on silicon,[16,17] the stamp can be utilized repeatedly without damaging the anti-sticking SAM.

The entire MOM tunneling diode is then created on the SAM-covered silicon stamp. First, a stack of 10 nm thick gold followed by 20 nm thick aluminum is deposited by vacuum evaporation through a shadow mask. This Au/Al stack

a)Electronic mail: bareiss@nano.ei.tum.de.

later serves as the top electrode of the printed diode. The reason for depositing a stack of two different metals is that this makes it possible to choose a first metal (gold) that provides minimum adhesion to the fluoroalkyl SAM (to facilitate delamination from the stamp) and a second metal (aluminum) that can be plasma-oxidized to create a thin, compact tunneling dielectric (AlO_x). This oxidation is performed by a brief oxygen-plasma treatment that increases the thickness of the native AlO_x layer on the aluminum surface from ~1.6 nm to ~3.6 nm.[18–20] In the next step, a stack of 30 nm thick gold (as the bottom electrode of the printed diode) followed by 4 nm thick titanium (to promote adhesion of the printed diode to the target substrate[21]) is deposited by vacuum evaporation through a second shadow mask. The titanium is allowed to oxidize and titanol surface groups are created by a UV and plasma treatment.[22,23]

Depositing the top and bottom electrodes through two different shadow masks makes it possible to also create a metal probe pad for each electrode to facilitate electrical characterization of the printed diodes. The active area of the diodes is the area by which the top and bottom electrodes overlap, as defined by the overlap of the designed shadow-mask features.

The completed diodes ($Au/Al/AlO_x/Au/TiO_x$), including the probe pads are then transfer-printed onto the target substrate, namely a silicon wafer covered with a 200 nm thick layer of thermally grown silicon dioxide (Fig. 1). Prior to printing, the surface of the target substrate is exposed to an oxygen plasma, treated with HCl to form silanol surface groups[24] and then dried with compressed nitrogen. Transfer printing is performed using an Obducat NIL 2.5 Nanoimprinter at a temperature of 200 °C and a pressure of 50 bar for 5 min. During the transfer process, the titanol and silanol surface groups on the stamp and on the substrate react to titansiloxanes under water release.[25] This reaction is strongly promoted by drying the surfaces prior to transfer and removing physisorbed water from the interface at 200 °C during the printing process.[26]

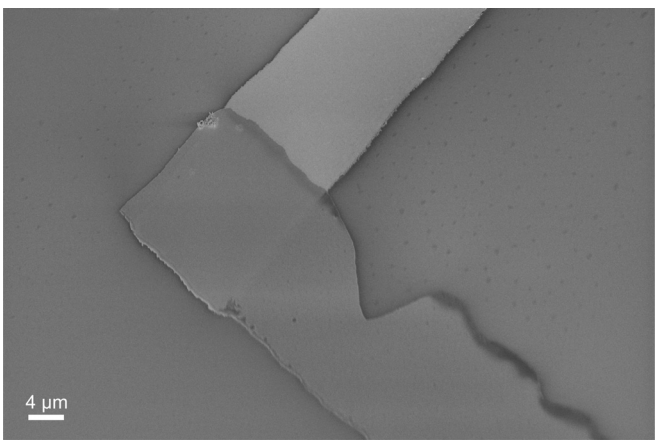

FIG. 1. SEM image of a printed MOM tunneling diode. The substrate is a thermally oxidized silicon wafer. The MOM diode is defined by the overlap of the gold electrode located at the bottom and the aluminum electrode located at the top. The tunneling dielectric is 3.6 nm thick AlO_x produced by plasma oxidation of the aluminum electrode prior to Au evaporation and printing. The entire MOM diode was transferred from a stamp onto the target substrate in a single printing step.

III. RESULTS AND DISCUSSION

Several hundred MOM diodes were transferred from the stamp to the target substrate in a single printing step in a normal laboratory (i.e., non-cleanroom) environment. In order to quantify the mechanical yield of the transfer process, we have imaged the printed devices by scanning electron microscopy (SEM) and counted the number of diodes that appear to have been transferred properly (like the diode shown in Fig. 1) and those that appear to have been damaged or transferred incompletely. By defining the transfer yield as the number of diodes that appear in the SEM images as properly transferred divided by the number of diodes that were originally created on the stamp, the transfer yield is 83%. In Fig. 2, the transfer yield is plotted as a function of the active area of the tunneling diodes, which ranges over three orders of magnitude. As can be seen, the mechanical transfer yield is above 70% over the entire range of diode areas. The transfer yield appears to be limited by particles on the surfaces that prevent substrate and stamp from making physical contact, leading to damage or incomplete transfer. This may explain why the transfer yield appears to decrease for larger areas where the probability for features to overlap with particles on the surface is expected to be higher. Clearly, under cleanroom conditions this problem would be substantially less severe. Atomic force microscope (AFM) measurements performed on the diode structures prior to printing and after printing confirm the structural integrity of the transferred diodes, as the total thickness of the devices does not change upon transfer.

These results show that by careful selection of materials and by adjusting the adhesive forces between the stamp surface and the top electrode as well as those between the bottom electrode and the surface of the target substrate, complete MOM diodes can be transfer-printed with large yield and excellent integrity.

The current-voltage characteristics of the transfer-printed MOM tunneling diodes are measured in ambient air at room temperature by contacting the printed top and bottom electrodes outside of the active diode area using probe needles and a parameter analyzer. In our measurements, the aluminum top electrode is set to ground potential, a positive

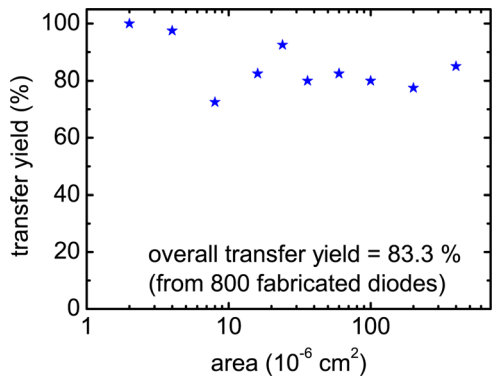

FIG. 2. (Color online) Mechanical yield of the transfer-printing process plotted as a function of the active area of the MOM tunneling diodes. As can be seen, a high yield of about 83% is obtained over a wide range of diode area.

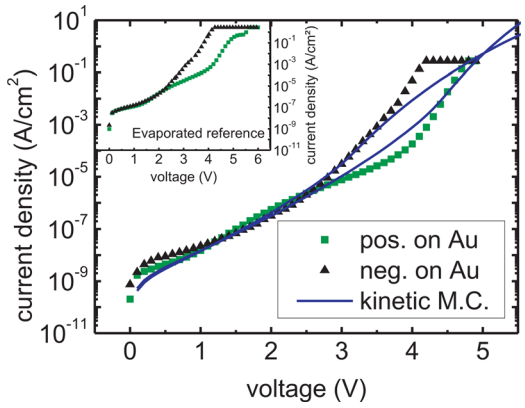

FIG. 3. (Color online) Current density through a transfer-printed MOM tunneling diode measured as a function of applied voltage for both polarities. The aluminum top electrode is set to ground potential, and the current is measured for positive (green data points) or negative (black data points) potentials applied to the gold bottom electrode. The lines represent the kinetic Monte Carlo simulation results using Eq. (1). In the inset the current-voltage curve of a transfer-printed MOM tunneling diode is compared to that of a diode based on the same material stack that was not transfer-printed.

or negative potential is applied to the gold bottom electrode and increased in small increments beginning from zero volts, and the current through the 3.6 nm thin plasma-grown AlO_x dielectric is measured as a function of the applied bias. In Fig. 3, the result of a current-voltage (I-V) measurement performed on a transfer-printed MOM diode is shown. In the graph, the absolute value of the measured current is plotted as a function of absolute value of the applied voltage, so that the asymmetry of the I-V curves can be easily evaluated. Symbols and lines represent experimental data and theoretical values, respectively. Comparing the slope of the I-V curve of a transfer-printed tunneling diode with that of a reference $Al/AlO_x/Au$ diode (not transfer-printed), it can be seen that the electron-transport mechanism in both structures is identical. Furthermore, the current densities in the transfer-printed diode and in the diode that was not printed are of the same order of magnitude, again confirming that the diodes are not damaged by the printing process.

An asymmetric slope of the two polarities was observed for larger voltages. For example, at a voltage of ± 3.5 V the current density due to electron injection from the gold electrode is around two orders of magnitude larger than for injection from the aluminum electrode. In order to identify the transport mechanism in the MOM diodes, the measured current was modeled using a kinetic Monte Carlo simulation.[27,28] Electron tunneling was found to be the dominant mechanism, due to the very small thickness of the dielectric (3.6 nm). The resulting current density j can be described by the Tsu-Esaki formula[29]

$$j = \frac{em_c k_B T}{2\pi^2 \hbar^3} \int_0^\infty P(E_t) ln \left[\frac{1 + exp\left(\frac{-E_t}{k_B T}\right)}{1 + exp\left(\frac{-eU - E_t}{k_B T}\right)} \right] dE_t, \quad (1)$$

where m_c is the conductivity mass for the injected electrons and $P(E_t)$ is the transmission coefficient for electrons with transversal energy E_t, calculated in the Wentzel-Kramers-Brillouin approximation. A close agreement with the experimental data, as shown in Fig. 3, is achieved by assuming an effective tunneling mass of $m_{ox} = 0.38 \cdot m_0$ for the aluminum oxide and tunneling barriers of 4.2 eV for the gold electrode, and 2.8 eV for the aluminum electrode. As the work function of gold is $\Phi_{Au} = 5.2$ eV, the extracted barrier height of 4.2 eV corresponds to a gold/aluminum oxide interface at the Schottky limit, i.e., without any barrier reduction due to charge transfer across the interface. Correspondingly, a barrier height of 3.2 eV would be expected for the aluminum barrier (taking $\Phi_{Al} = 4.2$ eV), which is slightly larger than the extracted value of 2.8 eV. This discrepancy may be due to the formation of a dipole layer produced by charge transfer between the aluminum electrode and interfacial gap states in the aluminum oxide, which is known to reduce the barrier height.[30,31] In general, the aluminum/aluminum oxide barrier height is known to strongly depend on, e.g., the growth method of the aluminum oxide.[32] For smaller voltages (0 to -2.8 V and 0 to $+4.2$ V) direct tunneling is the dominant transport mechanism. Minor deviations of the experimental data from the simulated curve for $|U| < 1$ V arise due to the applied voltage ramp, which causes transient relaxation currents and charging of defect states. These dominate over the steady-state leakage current.[33] For voltages more negative than -2.8 V or more positive than $+4.2$ V the slope of the I-V curves increases. This well-known characteristic feature arises due to the transition from direct tunneling to Fowler-Nordheim tunneling, that is, a transition from a trapezoidal to a triangular tunneling barrier. Consequently, the barrier thickness decreases as the applied voltage is increased. For current densities $|j| > 10^{-2}$ A/cm^2, irreversible degradation of the tunneling diode during the measurement and finally short-circuiting was observed.

These results show that the electrical properties of the MOM diodes, including the thin aluminum oxide layer, were not noticeably altered or degraded by the transfer-printing process.

Building upon the parameters determined so far, the identification of the permittivity of the printed aluminum oxide is of great interest with respect to, e.g., the discussion of aluminum oxide as *high-k* dielectric.[34] The permittivity of the aluminum oxide layer of the printed tunneling diode was determined by capacitance measurements in which the aluminum electrode was set to ground potential and a dc voltage modulated with a small ac bias was applied to the gold electrode. A capacitance density of $1.19 \cdot 10^{-6}$ F/cm^2 was measured for the 3.6 nm thick oxygen-plasma-grown aluminum oxide layer of the transfer-printed MOM tunneling diodes. Modeling the MOM diode as a conventional parallel-plate capacitor with aluminum oxide as the dielectric,[35] the permittivity can be calculated as

$$\epsilon = \frac{C \cdot d}{\epsilon_0 \cdot A}. \quad (2)$$

Here C/A is the capacitance per unit area, ϵ is the permittivity of the insulator, and d is the thickness of the insulator. For a dielectric thickness of 3.6 nm, a permittivity of 4.8 is

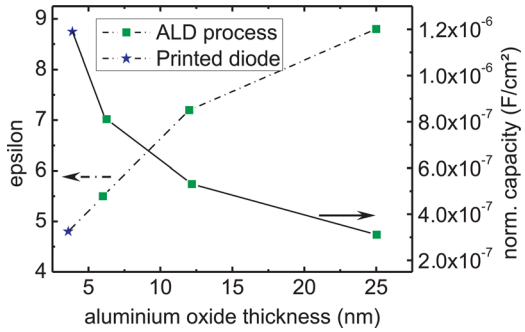

FIG. 4. (Color online) Measured capacitance of Al/AlO_x/Au diodes as a function of AlO_x thickness. The AlO_x film with a thickness of 3.6 nm was fabricated by a brief oxygen-plasma treatment that increases the thickness of the native AlO_x layer on the aluminum surface, while the thicker AlO_x films (6 nm, 12 nm, 25 nm) were deposited by atomic layer deposition (ALD). The permittivity calculated from the measurement data is also shown.

calculated, which is much smaller than the values around 9 that are typically presented in literature for bulk aluminum oxide.[36] However, it is also well-known that reducing the thickness of aluminum oxide is often accompanied by a reduction of the permittivity.[37] This can also be seen in Fig. 4, where the permittivity of the printed tunneling diodes was compared to diodes in which the metals were evaporated and the aluminum oxide was deposited by atomic layer deposition (ALD). Unlike plasma oxygen, ALD allows us to set the thickness of the AlO_x-layer to any value. As has been pointed out by Hickmott,[38] extracting the permittivity of the dielectric by using Eq. (2), especially for thin-film capacitors, leads to erroneous results, i.e., to an apparent reduction of ϵ. In fact, the observed decrease of ϵ for ultra-thin films is due to interfacial capacitances at the metal-insulator interfaces. Thus, Eq. (2) should be replaced by

$$\epsilon = \frac{1}{\epsilon_0} \cdot \frac{1}{\frac{A}{C} - \frac{A}{C_I}} \cdot d. \tag{3}$$

Here, C_I is an interface capacitance that depends on the metal contacts and is connected in series with the capacitance of the dielectric film. More precisely, C_I is not a property of the chosen metal-dielectric combination, but was found to depend on the deposition method of the metal electrode. It was concluded that the interface capacitance is not caused by the field penetration into the metal electrodes, as suggested by Mead.[39] Instead, it is due to the occurrence of interface states at the metal-dielectric interface, which depends on the deposition conditions of the metal electrodes.

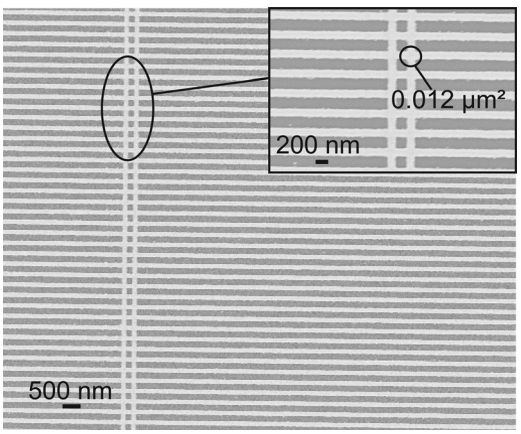

FIG. 5. Transfer-printed gold structures.

IV. CONCLUSION

In summary, we have reported on the fabrication and characterization of transfer-printed MOM tunneling diodes with gold and aluminum electrodes and a 3.6 nm thick, oxygen-plasma-grown aluminum oxide dielectric. We have shown that the dielectric retains its high quality during the transfer-printing process. Tunnel currents have been measured over eight orders of magnitude, including the transition from direct tunneling to Fowler-Nordheim-tunneling. The asymmetric behavior of the printed MOM diodes makes it possible to use them as rectifying devices. By comparison to a theoretical tunneling model, the static electronic properties of the diodes, i.e., the tunneling barrier heights and the tunneling effective mass, have been determined. Capacitance measurements performed on the printed devices indicate a permittivity of about 5 for the 3.6 nm thick aluminum oxide films, which is in line with previous investigations. As the mechanical yield of the transfer-printing process is above 80% (and even higher for smaller structures), we believe that transfer-printing is an efficient and economical process to cover large areas with rectifying MOM tunneling diodes without affecting the electrical performance of the diodes. The process can be further scaled down to arrays of nanometer-size MOM diodes to be transferred. This possibility is currently under investigation. In general, transfer-printing of structures at the nanometer scale is mostly limited by the grain size of the metal to be transferred. For example, gold is known to form clusters during metal deposition and consequently, a limit is achieved when trying to transfer very small structures where the gold on the stamp makes poor physical contact with the surface of the substrate. So far, the fabrication of gold structures with an area of 0.01 m^2 in a transfer-printing process is easily possible (see Fig. 5), however, scaling down to sizes below 50 nm is challenging. By exchanging gold with, for example, gold-palladium that features a smaller grain size than gold, smaller sizes should be possible to reach.

ACKNOWLEDGMENTS

The authors thank Omar Fakhr for fruitful discussions and Guido Hilgers for technical support. The research leading to these results has received funding from the Institute for Advanced Study (IAS), the International Graduate School for Science and Engineering (IGSSE) at the Technische Universität München, the European Community's Seventh Framework Programme (FP7/2007-2013) under Grant Agreement No. 228673, and the German Excellence Cluster "Nanosystems Initiative Munich" (NIM).

[1]I. Wilke, W. Herrmann, and F. K. Kneubühl, Appl. Phys. B **58**, 87 (1994).
[2]C. Fumeaux, J. Alda, and G. D. Boremann, Opt. Lett. **24**, 1629 (1999).

[3]J. A. Bean, B. Tiwari, G. H. Bernstein, P. Fay, and W. Porod, J. Vac. Sci. Technol. B **27**, 11 (2009).
[4]B. Tiwari, J. A. Bean, G. Szakmany, G. H. Bernstein, P. Fay, and W. Porod, J. Vac. Sci. Technol. B **27**, 2153 (2009).
[5]J. Alda, J. M. Rico-Garcia, J. M. Lopez-Alonso, and G. D. Boreman, Nanotechnol. **16**, 230 (2005).
[6]B. A. Slovick, J. A. Bean, P. M. Krenz, and G. D. Boreman, Opt. Express **18**, 20960 (2010).
[7]S. Harrer, S. Strobel, G. Scarpa, G. Abstreiter, M. Tornow, and P. Lugli, IEEE Trans. Nanotechnol. **7**, 363 (2008).
[8]J. Zaumseil, M. A. Meitl, J. W. P. Hsu, B. R. Acharya, K. W. Baldwin, Y. L. Loo, and J. A. Rogers, Nano Lett. **3**, 1223 (2003).
[9]Y. L. Loo, D. V. Lang, J. A. Rogers, and J. W. P. Hsu, Nano Lett. **3**, 913 (2003).
[10]Y. L. Loo, R. L. Willett, K. W. Baldwin, and J. A. Rogers, J. Am. Chem. Soc. **124**, 7654 (2002).
[11]J. G. Simmons, J. Appl. Phys. **34**, 1793 (1963).
[12]T. W. Hickmott, J. Appl. Phys. **108**, 093703 (2010).
[13]R. T. Weitz, U. Zschieschang, F. Effenberg, H. Klauk, M. Burghard, and K. Kern, Nano Lett. **7**, 22 (2007).
[14]M. Lafkioti, B. Krauss, T. Lohmann, U. Zschieschang, H. Klauk, K. v. Klitzing, and J. H. Smet, Nano Lett. **10**, 1149 (2010).
[15]R. Maboudian and R. T. Howe, J. Vac. Sci. Technol. B **15**, 1 (1997).
[16]W. Lee, R. Ji, C. A. Ross, U. Gösele, and K. Nielsch, Small **2**, 978 (2006).
[17]P. Russer, N. Fichtner, P. Lugli, W. Porod, J. A. Russer, and H. Yordanov, IEEE Microw. Mag. **11**, 58 (2010).
[18]R. T. Weitz, U. Zschieschang, A. Forment-Aliaga, D. Kälblein, M. Burghard, K. Kern, and H. Klauk, Nano Lett. **4**, 1335 (2009).
[19]U. Zschieschang, F. Ante, M. Schlörholz, M. Schmidt, K. Kern, and H. Klauk, Adv. Mater. **22**, 4489 (2010).
[20]H. Ryu, D. Kälblein, R. T. Weitz, F. Ante, U. Zschieschang, K. Kern, O. G. Schmidt, and H. Klauk, Nanotechnol. **21**, 475207 (2010).
[21]S. Strobel, S. Harrer, G. P. Blanco, G. Scarpa, G. Abstreiter, P. Lugli, and M. Tornow, Small **5**, 579 (2009).
[22]M. Nakamura, T. Aoki, and Y. Hatanaka, J. Mater. Res. **16**, 2 (2001).
[23]T. Ishigaki, H. Haneda, N. Okada, and S. Ito, Thin Solid Films **390**, 20 (2001).
[24]Y. L. Loo, D. V. Lang, J. A. Rogers, and J. W. P. Hsu, Nano Lett. **3**, 913 (2003).
[25]G. Kissinger and W. Kissinger, Phys. Status Solidi A **123**, 185 (1991).
[26]J. H. Anderson and K. A. Wickersheim, Surf. Sci. **2**, 252 (1964).
[27]G. Jegert, A. Kersch, W. Weinreich, U. Schröder, and P. Lugli, Appl. Phys. Lett. **96**, 062113 (2009).
[28]G. Jegert, A. Kersch, W. Weinreich, and P. Lugli, IEEE Trans. Electron Devices **58**, 327 (2011).
[29]R. Tsu and L. Esaki, Appl. Phys. Lett. **22**, 562 (1973).
[30]J. Robertson, J. Vac. Sci. Technol. B **27**, 277 (2009).
[31]J. Robertson, J. Vac. Sci. Technol. B **18**, 1785 (2000).
[32]T. W. Hickmott, J. Appl. Phys. **97**, 104505 (2005).
[33]V. K. Gueorguiev, P. V. Aleksandrova, T. E. Ivanov, and J. B. Koprinarova, Thin Solid Films **517**, 1815 (2009).
[34]T. D. Lin, H. C. Chiu, P. Chang, L. T. Tung, C. P. Chen, M. Hong, J. Kwo, W. Tsai, and Y. C. Wang, Appl. Phys. Lett. **93**, 033516 (2008).
[35]T. W. Hickmott, J. Appl. Phys. **87**, 7903 (2000).
[36]G. D. Wilk, R. M. Wallace, and J. M. Anthony, J. Appl. Phys. **89**, 5243 (2001).
[37]M. Groner, J. W. Elam, F. H. Fabreguette, and S. M. George, Thin Solid Films **413**, 186 (2002).
[38]T. W. Hickmott, J. Appl. Phys. **89**, 5502 (2001).
[39]C. A. Mead, Phys. Rev. Lett. **6**, 545 (1961).